The Effects of Stable Stratification on the Decay of Initially Isotropic Homogeneous Turbulence

By Stephen M. de Bruyn Kops[1] and James J. Riley[2]

[1]Department of Mechanical and Industrial Engineering,
University of Massachusetts Amherst, Amherst, Massachusetts, USA
[2]Department of Mechanical Engineering,
University of Washington, Seattle, Washington, USA

28 June 2018

We report on direct numerical simulations of the decay of initially isotropic, homogeneous turbulence subject to the application of stable density stratification. Flows were simulated for three different initial Reynolds numbers, but for the same initial Froude number. We find that the flows pass through three different dynamical regimes as they decay, depending on the local values of the Froude number and activity parameter. These regimes are analogous to those seen in the experimental study of **?** for the wake of a sphere. The flows initially decay with little influence of stratification, up to about one buoyancy period, when the local Froude number has dropped below 1. At this point the flows have adjusted to the density stratification, and, if the activity parameter is large enough, begin to decay at a slower rate and spread horizontally at a faster rate, consistent with the predictions of **?** and the scaling arguments of **?**. We refer to this second regime as the stratified turbulence regime. As the flows continue to decay, ultimately the activity parameter drops below about 1 as viscous effects begin to dominate. In this regime, the flows have become quasi-horizontal, and approximately obey the scaling arguments of **?**.

CONTENTS

1. Introduction

Stable density stratification can have a first-order effect on turbulence in the environment, such as in the atmosphere, the oceans, estuaries and lakes. Stable stratification allows for the propagation of internal gravity waves and, when strong, leads to the suppression of vertical motion and the modification of turbulence dynamics. In this paper we report on the impact of strong, stable stratification on initially homogeneous, isotropic turbulence. This allows us to study the effects of stratification on turbulence in one of its simplest forms, without the turbulence being sustained by a source of energy and without the effects of statistical non-homogeneity. The strength of the stratification can be indicated by a local (in time) Froude number, $Fr = 2\pi U/NL$, where U is an instantaneous r.m.s. velocity of the turbulence motions characterised by a length scale L, and $2\pi/N$ is the buoyancy period. The Froude number, the ratio of the buoyancy time scale $2\pi/N$ to the turbulence time scale L/U, is expected to decay as the flow decays. Of interest is how the dynamics of a flow, initiated at a somewhat high Froude number, are modified by the presence of stable stratification, the behaviour of the flow as the stable stratification becomes dominant, i.e., when $Fr < O(1)$, which is estimated to occur at about one buoyancy period after flow initiation (**???**), and the subsequent behaviour of the flow as viscous effects become important. We will refer to the turbulent flow regime when $Fr < O(1)$ as the 'strongly stratified' regime.

After the Froude number in a decaying flow has decreased to order one, the nonlinear dynamics are expected to have become significantly altered. For example, the vertical motion along with vortex stretching in the vertical are suppressed (**?**). In this regime, it is widely thought that the tendency towards the vertical decoupling of horizontal motions and subsequent shearing become an important instability and turbulence-generating mechanism, as suggested by the physical arguments of **?** and the scaling analysis of **?**. These arguments, along with the results from laboratory experiments [e.g., **??**], indicate that in the strongly stratified regime the flow becomes highly anisotropic, and that it is useful to distinguish, for example, the vertical and horizontal integral scales of the r.m.s. horizontal velocity U_h, i.e., L_h and L_v, respectively. The strongly stratified regime will then be defined when $Fr_h = U_h/NL_h$ is small, i.e., when the ratio of the buoyancy period to the horizontal advection time scale L_h/U_h is small. On the other hand, the arguments of **?** and **?** predict that $Fr_v = U_h/NL_v$ will remain of order 1.

For the most part we narrow our focus to the strongly stratified regime when the Reynolds number $Re_h = U_h L_h/\nu$ is large enough so that the buoyancy Reynolds number $\mathcal{R} = {Fr_h}^2 Re_h$ is greater than order one, although we will also address the regime where $\mathcal{R}$ is small. Here ν is the kinematic viscosity. The inequality $\mathcal{R} > O(1)$ implies that the flow is strong enough to continue to cause smaller-scale instabilities and turbulence (**??**).

The decay of homogeneous turbulence subject to stable density stratification has been the subject of a number of laboratory experiments, numerical simulations, and theoretical analyses. In the laboratory, several studies have been carried out by towing a grid through a salt-stratified water tank (**????**), flowing water past a grid in a salt-stratified flume (**??**), or flow past a grid in a temperature-stratified wind tunnel (**??**). In each case detailed measurements were made downstream of the grid to determine the flow properties and its evolution. These experiments each produced an approximation to homogeneous decay; it must be realised, however, that the laboratory flows are initiated in a somewhat different manner than those in the numerical simulations reported here. In the laboratory experiments the turbulence is generated while the stable stratification is already present, while in our simulations isotropic turbulence is first developed and subsequently the stable stratification is applied.

Considerable insight into the effects of stable stratification on turbulent flows has been gained from these experimental studies. The results for the energy decay rate, however, which is one of the principal motivations of the present study, are mixed. For example, **?** towed a biplane grid at constant speed in a tank uniformly salt-stratified for a range of mesh Froude numbers, $Fr_M = 2\pi U/NM \approx \infty, 80$, and 40; here U is the towing speed and M the mesh spacing. He found that the kinetic energy decay rate increased from about $(x/M)^{-1.3}$ for the non-stratified case to $(x/M)^{-1.65}$ for the stratified cases. In addition the potential energy decayed as $(x/M)^{-1.5}$, and attained a value of about 50% of the total kinetic energy, indicating that the stratification was playing a significant role in the overall dynamics. Liu also found that the time-local Froude number Fr decays as approximately $(x/MF_M)^{-1}$, as predicted by **?**, and became $\mathcal{O}(1)$ at $Nt/2\pi = x/MF_M \approx 1$, indicating the effects of stratification became strong in about one buoyancy period. **?** also studied the turbulence behind a towed grid; however, their grid was not biplane, but consisted of the wakes of only vertical plates to eliminate enhanced internal waves which would be generated by horizontal plates. In particular they examined the later time behaviour of the turbulence, where quasi-horizontal motions were observed after the collapse of the three-dimensional turbulence. Remarkably, they observed that the turbulent kinetic energy decay rate was the same as for the non-stratified case. The decay mechanism, however, appeared to be different, as strong vertical shearing developed in the horizontal motions. In wind tunnel experiments, because of the limitations of wind tunnel length, **?** were only able to explore turbulence decay for about one buoyancy period. They did find, however, contrary to the results of **?** and **?**, that stable stratification inhibited the turbulence decay. Similarly, in their water channel experiments, **?** also found that stable stratification inhibited the decay of the turbulence. Therefore, from these laboratory experiments, it is unclear whether stable stratification might enhance or inhibit turbulence decay, and what the corresponding mechanisms might be.

The effects of stable stratification on turbulent wake decay were obtained from the laboratory experiments of **?** and **?** conducted in the wake of a slender, axisymmetric body and of a sphere, respectively. In both cases the model was towed at constant speed through a uniformly stratified water tank. The experiments of **?** were carried out in a Reynolds number range of $2 \cdot 10^4 \leq Re_D \leq 3 \cdot 10^4$ and a Froude number range of $23 \leq F_D \leq 120$, where $Re_D = UD/\nu$ and $F_D = 2\pi U/ND$; U and D are the towing speed and the diameter defined from projected area of the model, respectively. It might be expected that the wake of a slender object or a sphere would decay faster for experiments with stable stratification than for ones without stratification, since internal wave radiation (**?**) would lead to additional decrease in the energy in the wake region. **?** found, for example, that the turbulence behaviour for stratified cases was about the same as for non-stratified cases up to about one to two buoyancy periods after the initiation of the turbulence. At that point, however, the turbulence in the streamwise direction began to decay more slowly, while that in the vertical direction decayed faster. **?** performed experiments for Reynolds numbers in the range $1.0 \cdot 10^4 \leq Re_D \leq 2.3 \cdot 10^4$, and Froude numbers in the range $31.4 \leq F_D \leq 753$, where now the Froude number is defined as $F_D = U/ND$. In a similar vein, Spedding found that at about one-third of a buoyancy period downstream from the sphere, the decay rate of the centerline mean velocity decreased from the non-stratified rate of $(Nt)^{-2/3}$ to $(Nt)^{-1/4}$. The regime with the slow decay rate he referred to as the non-equilibrium regime. Furthermore he found that, at about ten buoyancy periods, the decay rate increased to about $(Nt)^{-3/4}$. He referred to this as the quasi-two-dimensional regime, where a quasi-horizontal vortex wake, but with variation in the vertical, was clearly apparent in visualizations, as seen in previous experiments (**?**).

? performed a laboratory study meant to simulate 'pancake' vortices similar to what is seen in the quasi-horizontal wakes of **?** and **?**. A vertically uniform vortex pair is generated with vertical flaps in a salt-water stratified tank. The generated vortices were allowed to pass through a horizontal slot, narrowing their vertical range. **?** found two regimes for the time-dependence of the vertical scale L_v of the vortices; in both cases the value of $\mathcal{R}$ was fairly small. In particular, they found for one of their cases that $L_v = L_h Re_h^{-1/2}$, similar to the results of **?** when $\mathcal{R}$ was small. They discussed these results in terms of the scaling analysis introduced by **?**, but with the effect of viscosity included. These results will be discussed further in §3.2.

Many numerical simulations have been conducted to understand decaying stratified turbulence, beginning with the work of **?**. They initiated their simulations by allowing the turbulence to develop nonlinearly without stratification, and then applying the density stratification. They found that stratification introduced a wave-like character in the flow field, with exchanges of kinetic and potential energies and the development of counter-gradient buoyancy fluxes, something also observed in the laboratory by **?**. Contrary to some of the laboratory experiments mentioned, but qualitatively consistent with others, they found that the stable stratification slightly inhibited the total energy decay rate. They found that stratification modified the nonlinear dynamics by inhibiting vortex stretching and suppressing the vertical component of the kinetic energy. Finally they introduced scaling arguments to explain the quasi-horizontal motions observed in the laboratory data.

A number of other simulations of homogeneous, stably-stratified turbulence have been performed, using different initial conditions and for different research purposes. For example **?**, and **?** initiated or forced their flows with vertically independent, horizontal motions, but with very small amplitude, three dimensional noise added, in order to study the effects of stable density stratification on the three-dimensional breakdown of the flows. They found the two-dimensional motions collapsed into thin horizontal layers, which had been suggested by the heuristic arguments of **?** and was later predicted by the scaling analysis of **?**.

With the introduction of larger computers, various initial conditions have been used to understand particular aspects of the strongly stratified flow regime. For example, **?** considered an initial Taylor-Green configuration, conceived of as an idealisation of the quasi-two-dimensional regime downstream of a grid or a sphere. Although the simulations were initialised with overall Richardson numbers well above one, they found that the Richardson numbers sharply decreased in time until the flows became unstable due to the vertical shearing of the horizontal motions, as suggested by **?**. They also observed a -5/3 behaviour of the horizontal wave number spectrum, something ultimately predicted by **?**. In contrast, **?** examined decaying homogeneous turbulence but starting with isotropic, random-phase velocity fields. They found results consistent with the scaling arguments of **?** as long as the buoyancy Reynolds number $\mathcal{R}$ was high enough. **?** employed a similar initialization to study the decay of homogeneous, stratified turbulence. They introduced a scaling analysis of the vorticity equation, emphasizing the importance of the vertical shearing of the horizontal motion, as argued by **?** and **?**. They found that the dissipation scaling $\epsilon \sim U_h^3/L_h$ was valid for the entire range of $\mathcal{R}$, and also found agreement with the -5/3 horizontal spectral range, as argued by **?**. Finally, they found that, once the effects of stratification became strong, then Fr_v remained approximately a constant of order 1. **?** considered forced, strongly stratified turbulence for a range of Froude and Reynolds numbers. They found two regimes depending on the value of $\mathcal{R}$. For large $\mathcal{R}$, $L_v \sim U_h/N$,

i.e., $Fr_v \sim 1$. For small $\mathcal{R}$, however, they found that $L_v \sim L_h/Re_h^{1/2}$. Furthermore they found horizontal wave number spectra somewhat consistent with the predictions of **?**.

Using fully nonlinear numerical simulations, **?** simulated the experiments of **?** for the wake of a sphere for a range of Reynolds numbers. In particular they found that the temporal extent of the non-equilibrium regime defined by Spedding increased as the Reynolds number increased. This prolongation was found to be due to instabilities in inclined shear layers, whose thicknesses decreased as the Reynolds number increased.

? addressed the issue of the decay of homogeneous, strongly stratified turbulence ($Fr < \mathcal{O}(1)$) using the theoretical approach of **?**. Studying the decay of homogeneous, isotopic turbulence, **?** assumed that the kinetic energy spectrum behaves as $E(k) \sim k^2$ as $k \to 0$, and predicted that

$$U^2 \sim t^{-6/5}\,, \quad L \sim t^{2/5}\,,$$

where U is the instantaneous r.m.s. velocity of the turbulence motions with integral length scale L. Following Saffman's approach, **?** was able to establish that, for homogeneous, strongly stratified turbulence, $U_h^2 L_h^2 L_v \approx$ constant. Here U_h and L_h are characteristic horizontal r.m.s velocity and horizontal integral scales, and L_v is a characteristic vertical integral scale. Then, using the additional constraint $U_h/NL_v \sim 1$ (**?**), he predicted that

$$U_h^2 \sim t^{-4/5}\,, \quad L_h \sim t^{3/5}\,, \quad L_v \sim t^{-2/5}\,. \tag{1.1}$$

Therefore Davidson predicted a slower decay of the horizontal r.m.s. velocity due to stable stratification. On the other hand he predicted a faster growth of the horizontal integral scale of the horizontal r.m.s. velocity, but a decay with time of the vertical integral scale of the horizontal r.m.s. velocity.

In the next section the numerical approach to the simulations will be outlined, followed by our simulation results in section 3. In that section we will discuss, in particular, the effects of stratification on the decay characteristics of the flow, on the flow energetics, on the dissipation rates and mixing efficiency, and on energy spectra. We will also address the modification of these results as the effects of viscosity become important. Finally, in section 4 we will further discuss our results and present our conclusions.

2. Numerical Methodology

In the introduction, we narrowed our scope of interest to flows with initially high Froude number that decay until $Fr < O(1)$ but with $\mathcal{R} = {Fr_h}^2 Re_h$ high enough to sustain turbulence. To study such flows we consider three decaying stratified flow simulations which differ only in Reynolds number so that each transitions through about the same range of Froude numbers but with differing values of $\mathcal{R}$. Corresponding to each stratified case is a nonstratified simulation initialised with exactly the same fields. So six simulations are used for this study but, since the nonstratified cases are used only to provide reference for the stratified cases, we refer to the simulations in terms of three cases, each with a stratified and nonstratified simulation.

To create the initial velocity fields, simulations with no stratification are forced to match Pope's model spectrum with his parameters $p_0 = 2$ and $c_L = 6.78$ (**?**, equation 6.247). This is accomplished by applying a deterministic forcing schema similar to that of **?** (c.f. **?**). For this initialisation process, the methodology is the same as that discussed in **?**. In short, a pseudospectral method is used to solve the discretised Navier-Stokes equations. The third-order Adams Bashforth method with pressure projection is used to advance the equations in time, as suggested by **?**. The fields are fully dealiased using the 2/3-method of truncation.

The forcing schema involves solving overdamped, second-order ordinary differential equations for the kinetic energy in each wave number shell in order to converge the simulated spectrum to a target spectrum. Since the forcing responds to the evolving flow field, convergence is achieved in the quasi-stationary sense. Once statistical stationarity is observed, forcing is turned off and the flow is allowed to relax, still with zero buoyancy force, until power-law decay is observed. The virtual origin for power law decay is designated $\hat{t}_0$. Next we define the dimensionless time $t \equiv (\hat{t} - \hat{t}_0)/\hat{t}_{LE} = 1$ as the starting point for the simulations. Here, time is nondimensionalised by the large-eddy advective time scale $\hat{t}_{LE} = \hat{L}/\hat{U}$ with $\hat{L}$ the integral length scale of the turbulence at $t = 1$ and $\hat{U}$ the corresponding r.m.s. velocity. The initial velocity fields for the stratified simulations, and for the corresponding nonstratified flow simulations, are those at $t = 1$.

Note that while the initialisation of the three simulation cases started by forcing them all to the same target spectrum, the velocity fields are different locally and the Reynolds numbers are different; so the simulations decay at different rates and have slightly different virtual origins. In order to easily compare the three cases, we have introduced the notation $\hat{(\,)}$ to denote a dimensional quantity. Since this notation can be cumbersome to read, it was not used in §1.

There are two time scales of interest in decaying stratified flows. One is the advective time scale, which in dimensional terms is $\hat{t}_{LE} = \hat{L}/\hat{U}$. The second time scale is the buoyancy period, which in dimensional terms is $\hat{T}_B = 2\pi/\hat{N}$. It is usual to examine the flow variables as functions of t, i.e., time scaled by the advective time $\hat{t}_{LE}$. It is sometimes useful, however, to observe the flows in terms of the number of buoyancy periods after stratification has been applied, that is, in terms of T defined by

$$T = \left(\hat{t} - \hat{t}_0 - \frac{\hat{L}}{\hat{U}} \right) \Big/ \hat{T}_B = \frac{t-1}{Fr} \ .$$

Both times will be used in presenting our results.

To impose stratification at $t = 1$, two changes are made to the simulations. First, a uniform, time-invariant, stable ambient density gradient with magnitude $d\overline{\hat{\rho}}/d\hat{z}$ is applied. Note that, from this density gradient, a density scale can be defined by $\hat{\rho} = \hat{L} d\overline{\hat{\rho}}/d\hat{z}$. Second, the governing equations being solved are modified to satisfy the non-hydrostatic Boussinesq assumption. Thus, after density stratification has been applied, the dimensionless governing equations are:

$$\frac{\partial \vec{v}}{\partial t} + \vec{v} \cdot \nabla \vec{v} = -\left(\frac{2\pi}{Fr} \right)^2 \rho \, \vec{e}_z - \nabla p + \frac{1}{Re} \nabla^2 \vec{v} \tag{2.1a}$$

$$\nabla \cdot \vec{v} = 0 \tag{2.1b}$$

$$\frac{\partial \rho}{\partial t} + \vec{v} \cdot \nabla \rho - w = \frac{1}{RePr} \nabla^2 \rho \ . \tag{2.1c}$$

Here $\vec{v} = (u, v, w)$ is the velocity vector in the Cartesian coordinate system $\vec{x} = (x, y, z)$ with z oriented in the vertical direction, ρ and p are the density and pressure deviations from their ambient values, and $Pr = \hat{\nu}/\hat{D}$ is the Prandtl number, which is taken to be unity; $\hat{\nu}$ is the kinematic viscosity and $\hat{D}$ the density diffusivity. The equations have been non-nondimensionalised by the length scale $\hat{L}$, the time scale $\hat{t}_{LE}$, and the density scale $\hat{\rho}$ defined above. In the present simulations, $\hat{L}$ is taken to be $\hat{L}_h$, the longitudinal integral scale in the horizontal direction at $t = 1$. The nominal Reynolds number Re, Froude number Fr, and time scaling are defined by the flow conditions at the instant

stratification is applied ($t = 1$) as

$$Re = \frac{\hat{U}\hat{L}}{\hat{\nu}} \quad , \quad Fr = \frac{2\pi\hat{U}}{\hat{N}\hat{L}} \quad , \quad t = \frac{\hat{t} - \hat{t}_0}{\hat{t}_{LE}} \ ,$$

where $\hat{N} = \left[-(\hat{g}/\hat{\rho}_0)/(d\overline{\hat{\rho}}/d\hat{z})\right]^{1/2}$ is the buoyancy frequency, $\hat{g}$ is the gravitational acceleration in the $-z$ direction, and $\hat{\rho}_0$ is the density at a reference elevation $\hat{z}_0$. In terms of dimensionless quantities, the total density is

$$\rho_t = \rho_0 + (z - z_0) + \rho \ .$$

Parameters for the three stratified flow simulations considered are listed in table 1. The only difference in input parameters between the simulations is the Reynolds number and, hence, there are different requirements on the small-scale numerical resolution for each simulation. The integral Reynolds number Re_h and Froude number Fr_h are defined in terms of the r.m.s. horizontal velocity and horizontal velocity longitudinal integral scale. The initial Froude number for each case is 2.0, and the initial Reynolds numbers are 160 (Case I), 653 (Case II), and 2325 (Case III). The resolution of the simulations was chosen to enable simulating for long times (over more than 100 buoyancy periods) while satisfying the large-scale and small-scale resolution requirements identified by **?** and **?**, respectively. In particular, the domain is at least 20 times the horizontal integral length scale, even at late times, and the maximum wave number, after application of the dealiasing filter, times the Kolmogorov length scale is at least unity at early times. Note that the grid spacing Δ is the effective size after dealiasing.

3. Simulation Results

Some qualitative idea of the behaviour of the stratified flows as they decay can be seen in figure 1, which gives lines of constant total density on a vertical plane at several different early times for Case III. For ease of visualisation, only shown is a section of a vertical plane consisting of the upper 1/32 and the leftmost 1/16 of the computational grid. Of course initially the lines are horizontal, as the initial density fluctuation is 0. Early on in the simulation, at $T = 0.5$, where time here is measured in buoyancy periods, the lines become highly contorted, with considerable density overturning, much as would be the case for a flow without gravity. As the flow evolves, however, the lines become more horizontal and, by $T = 4.0$, only a few regions of overtuning are evident. The effects of stably stratification on the flow are clearly evident. Figure 2 contains grey scale plots, for the same conditions as in Figure 1, of the turbulence activity parameter Gn, to be defined in 3.1.6 below, which gives an indication of the strength of the turbulence. Although at $T = 0.5$ the effects of stable stratification are little noticeable, by two and especially four buoyancy periods a quasi-horizontal nature and a patchiness of the turbulence are clearly evident.

3.1. *Early and intermediate time results*

We first address the early and intermediate time development of the stratified flows, defined here as when the effects of viscosity play only a secondary role in the development of the flows. We will find later (see §3.2 below) that this flow regime extends to about 2 buoyancy periods for Case I, 4 buoyancy periods for Case II, and about 11 buoyancy periods for Case III.

		Case I		Case II		Case III		Case IV	
		$t=1$	$t=10$	$t=1$	$t=10$	$t=1$	$t=10$	$t=1$	$t=6$
Integral Reynolds number	Re_h	160	201	653	817	2325	2844	2325	2973
Taylor Reynolds number	Re_λ	56	62	158	136	335	271	335	286
Activity parameter	Gn	12.63	0.14	25.98	0.61	65.40	2.36	65.40	1.43
Horiz. Froude number	Fr_h	2.00	0.25	2.00	0.27	2.00	0.30	1.00	0.24
Horiz. domain size to integral length	$\mathcal{L}_h/L_h$	71.3	21.8	76.9	25.2	85.9	30.3	85.9	39.0
Integral length to grid spacing	L_h/Δ	28.7	93.9	53.3	162.5	95.3	270.1	95.3	209.9
Max. wave number $\times$ Kolm. length	$\kappa_{max}L_k$	1.5	4.8	1.5	3.8	1.1	2.5	1.1	2.0
Grid spacing / Kolm. length	Δ/L_k	1.8	0.6	1.9	0.8	2.6	1.1	2.6	1.4
Vert. domain size to horiz. domain size	$\mathcal{L}_v/\mathcal{L}_h$	0.5		0.5		0.5		0.5	
Horiz. grid points	N_x,N_y	2048		4096		8192		8192	
Vertical grid points	N_z	1024		2048		4096		4096	

TABLE 1. Simulation parameters and metrics at two times for each stratified simulation. There is a corresponding unstratified simulation with identical conditions at $t = 1$. 'Integral length' is the average of the two horizontal longitudinal integral length scales each computed as recommended in Appendix E of **?**.

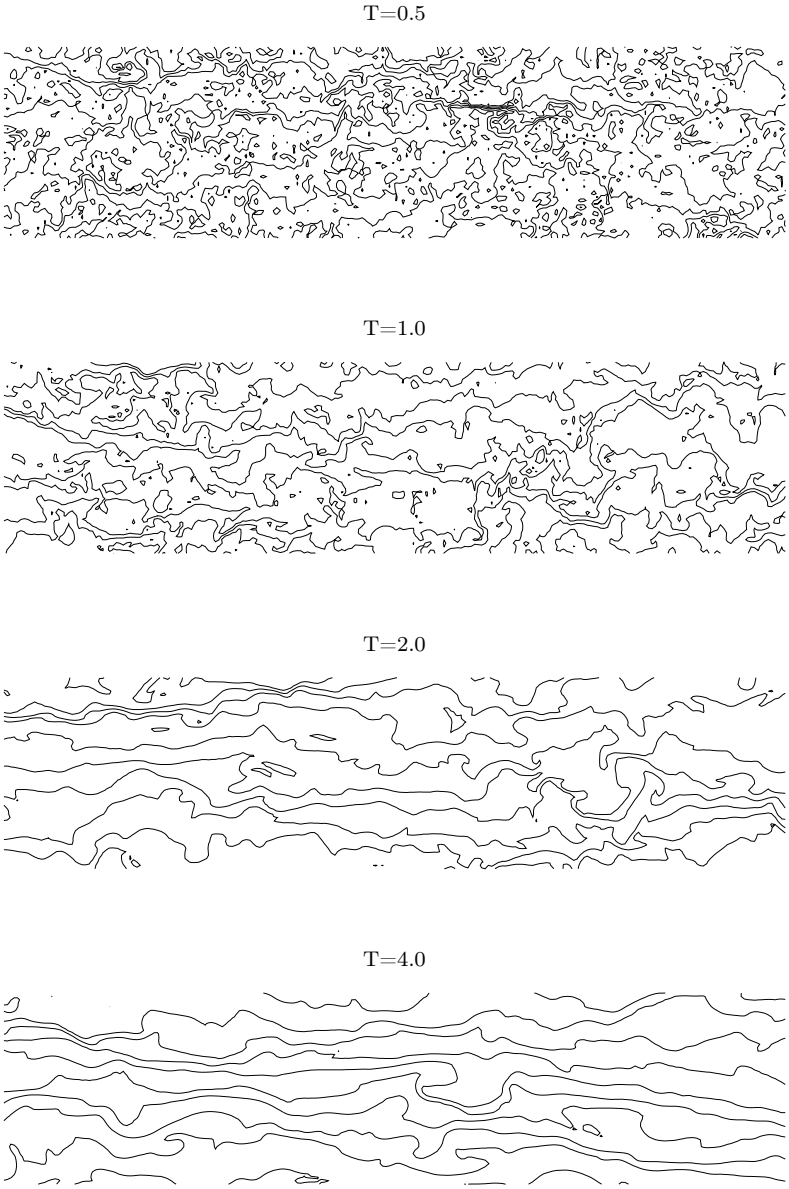

FIGURE 1. Lines of constant total density on a vertical plane at several times for Case III. The upper 1/32 and the leftmost 1/16 of the domain is plotted.

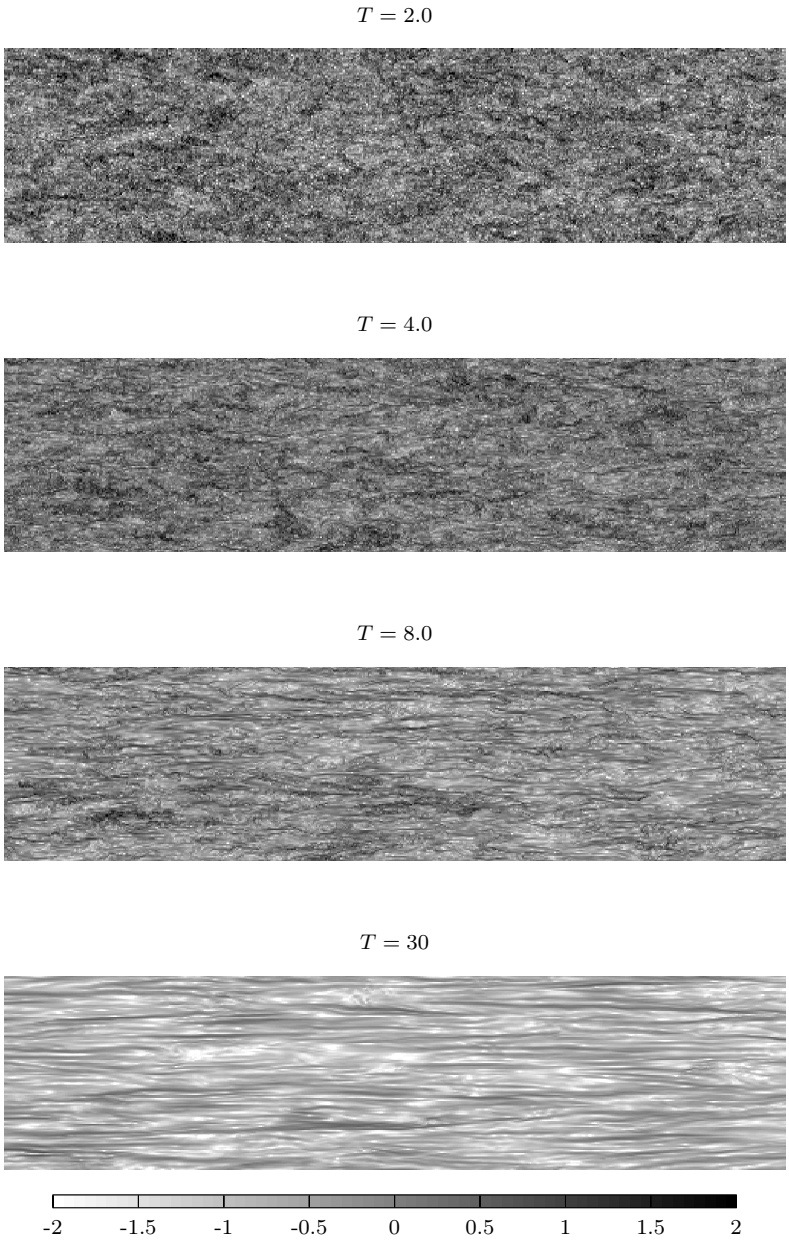

FIGURE 2. $\log_{10}(Gn)$ on a vertical slice of Case III at various times. Only the upper 1/4 and left 1/2 of the domain is plotted.

3.1.1. *Power-law scaling and the virtual origins*

We begin our study by examining the decay of non-stratified turbulence for the three cases used as the initial conditions for the stratified cases, and refer the reader to **?**, **?**, and **?**, and the references therein, for theoretical and experimental studies of the decay of homogeneous, isotropic turbulence. A primary interest here is in the power-law decay relationships

$$u' \propto t^{-n}$$
$$L' \propto t^{m}\,,$$

where u' is the volume-averaged r.m.s. value of any of the velocity components, t is measured from a virtual origin t_0, and L' is the corresponding integral length scale, either longitudinal or transverse. If L' is proportional to ${u'}^3/\epsilon$, where ϵ is the volume-averaged dissipation rate of turbulence kinetic energy, then $m = 1-n$, although with laboratory or numerical simulation data for homogeneous, isotropic turbulence this relationship may not be observed exactly and many studies report only n (c.f. **?**). From the plots by **?** of n as a function of Reynolds number based on data from numerous sources, and from Saffman's theory (**??**), we expect $n \approx 0.6$ for the current simulations.

The interdependence of n and the virtual origin t_0 makes the calculation of these parameters and their corresponding uncertainties dependent on how the curve fitting is carried out, which is beyond the scope of this paper. Here our immediate objective is to establish that the non-stratified simulations exhibit power-law decay with a value of n consistent with that in the literature. Figure 3 indicates that this is the case. In the plots u', v', and w' denote the r.m.s. velocities in the x, y, and z directions, respectively, with z in the vertical direction. In the figure, the symbols representing the non-stratified flow data lie on curves corresponding to $n = 0.56$, 0.56, and 0.55 for Reynolds numbers 160 (Case I), 600 (Case II), and 2325 (Case III), respectively. These are consistent with the expectation that $n \approx 0.6$.

3.1.2. *Power-law scaling in the stratified flows*

Also plotted in figure 3 are the r.m.s. velocities and in figure 4 the integral length scales for the three stratified cases, the latter which are computed as recommended in Appendix E of **?**. The notation L_{ux} denotes the integral length scale of u in the x-direction, and similarly for the other length scales.

Consider first the r.m.s. velocities, which are plotted in figure 3. There is an adjustment immediately following the onset of stratification at $t = 1$, the abruptness of which can be observed in the evolution of the r.m.s. density in figure 5. By about $t = 3$ ($T = 1$, *i.e.*, one buoyancy period), the decay rates for u' and v' begin to deviate from their non-stratified values, and settle into power-law decay rates which are less than the non-stratified values. Furthermore, from figure 3d, it is seen that the decay rates are very weakly dependent on the Reynolds number, with the lowest decay rate observed for Case III, the case with the highest Reynolds number. This observed decrease in the decay rate due to stable stratification is consistent with the prediction of **?**, although the decay rates are slightly less (in absolute value) than his estimate of $t^{-0.4}$. The reduction in decay rate is also qualitatively consistent with the experiments of **?**, **?**, **?** and **?**, and with the observations of **?** who, in simulations forced to maintain constant energy in a narrow band of small wave numbers, observed that stronger stratification slightly reduces the dissipation rate. These results are inconsistent with the laboratory experiments of **?**, however, who finds a decay rate of the horizontal velocities of about $n = 0.825$ with stratification, *faster* than the rate of 0.65 for his non-stratified case. It is also inconsistent with the results of **?** who

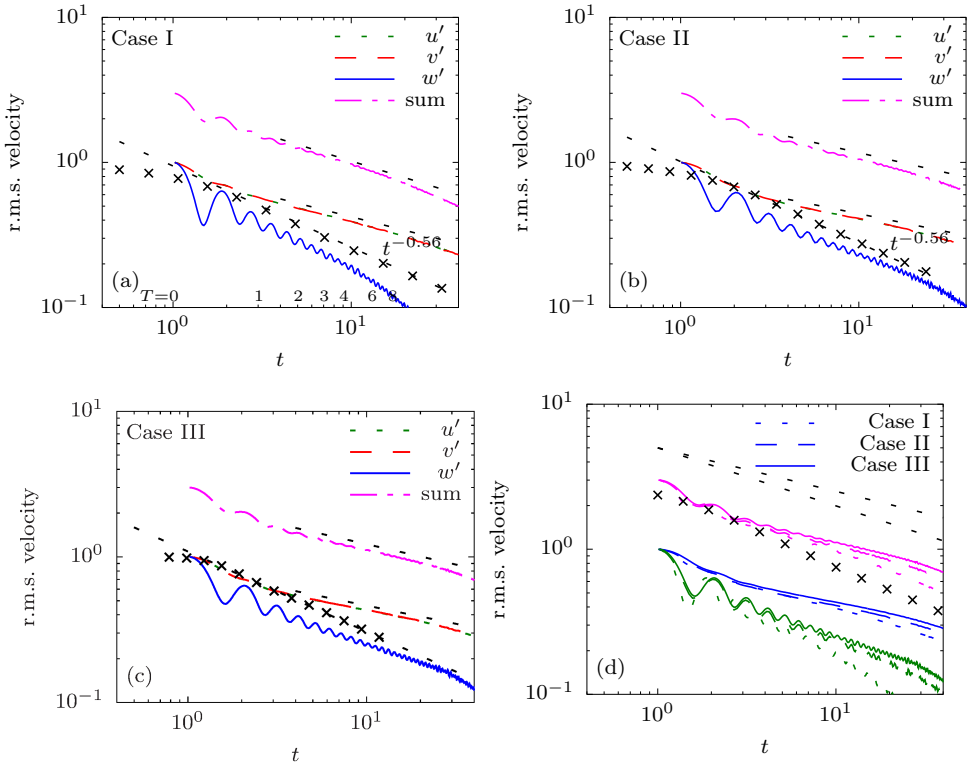

FIGURE 3. R.m.s velocities versus time t. Symbols are for non-stratified cases (only for Case I in panel (d)). The reference slopes are determined by least-squares fits to the logarithms of the data in the adjacent lines or symbols.

found the decay rate of about $n = 0.65$ for all their nonstratified and stratified cases. Note that, in our simulations with stable stratification, after some initial adjustment, w' decays at almost the same rate as with no stratification for cases II and III. When the Reynolds number is low (Case I at later times) though, w' decays faster with stratification than without. This is most easily observed in figure 3d.

In figure 4 it is seen that the growth rates of all the horizontal integral length scales are enhanced by the density stratification. The growths of the vertical integral scales of u', however, are so strongly affected by the stratification as to become negative at later times for cases Case II and Case III. Both of these results are qualitatively consistent with the predictions of **?**. The result for the vertical scales is consistent with the suggestion by **?** that, as the effects of stratification become important, the vertical shearing of the horizontal velocities increases. It is also consistent with the scaling analysis of **?**. The fact that all but the vertical lengths are larger in the stratified cases than in the non-stratified cases does not necessarily mean that coherent structures are larger, but rather that the small scales are suppressed. This will become more apparent when we discuss energy spectra. Note that the strong oscillations in the integral length scales for the vertical velocities are caused by the oscillatory exchanges of kinetic and potential energies, as the flows respond to the stable stratification. This is seen in the oscillations in w' in figure 3, and will become more clear when plots of the time dependence of the potential energy and the buoyancy flux are examined in figures 5 and 8. Also note that, when

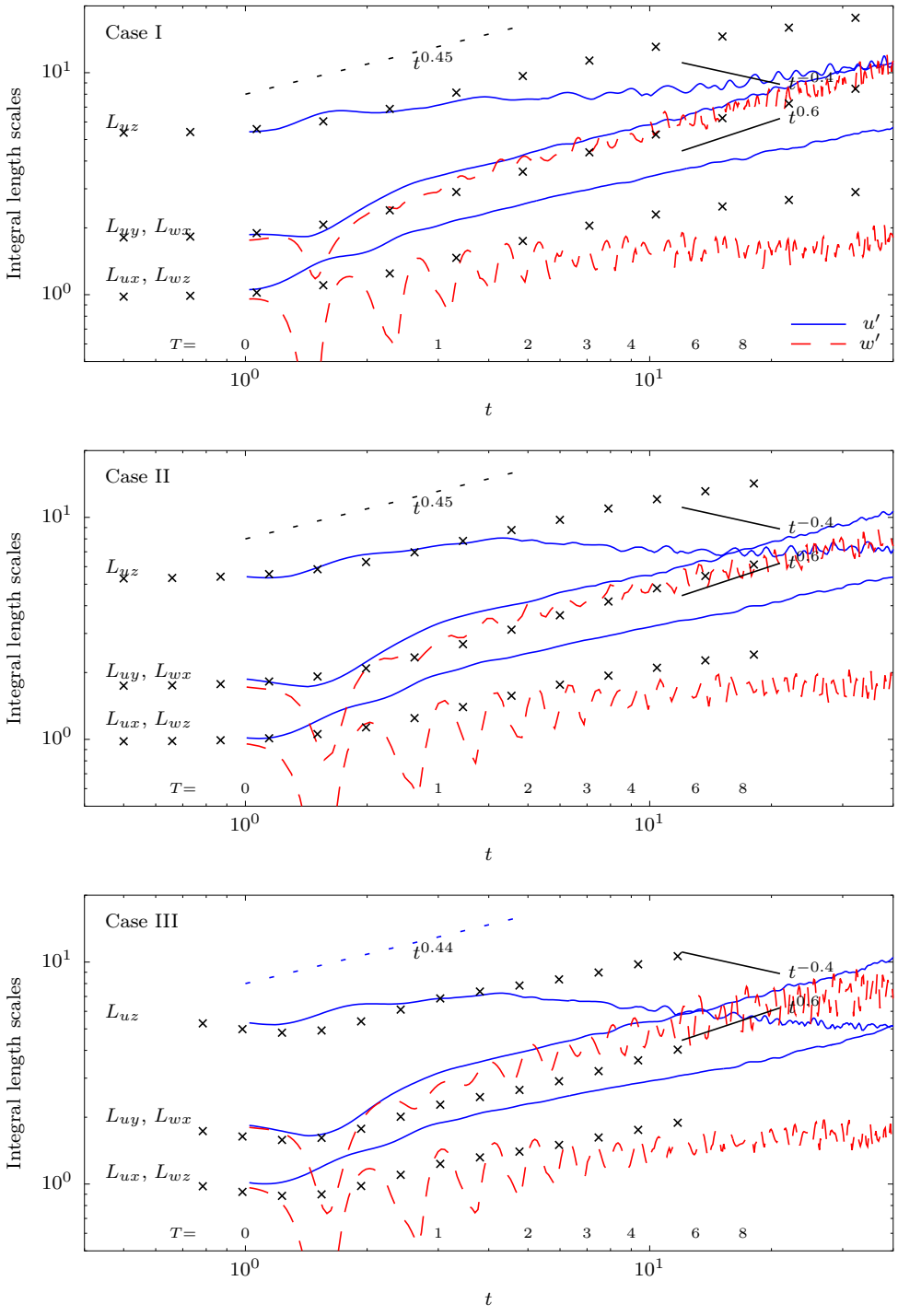

FIGURE 4. Integral lengths versus t. The longitudinal scales are plotted true and the others are offset vertically in increments of half decades. The symbols are for non-stratified cases. The dashed-line reference slopes are $1-n$ from the non-stratified simulations. The solid-line reference slopes are as derived in **?**.

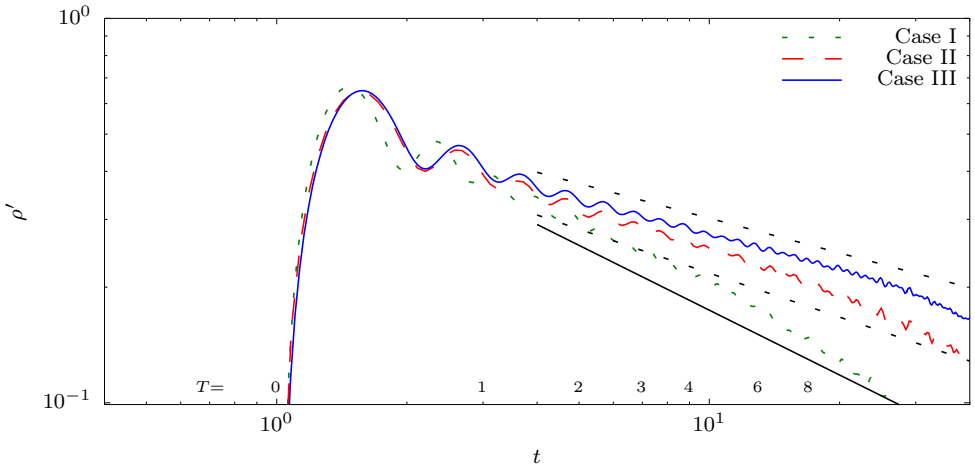

FIGURE 5. R.m.s. of the fluctuating density ρ' versus time t. The dashed reference slopes are from the total r.m.s. velocities in the stratified cases. The solid reference slope is for the r.m.s. velocity in the unstratified case I.

these oscillations are averaged out, the growth rates of L_{wz} are almost the same as for the non-stratified case.

The r.m.s of the density fluctuations provides yet another measure of the decay rate of stratified turbulence. For a passive scalar ϕ in isotropic turbulence with $u' \propto t^{-n}$, similarity analysis and data indicate that $\phi' \propto t^{-n}$ as well (c.f. **?**). Since the stratified flows exhibit different decay rates for the horizontal and vertical velocities, we might not expect the decay rate of the scalar fluctuations to agree with that of any single velocity component. From figure 5, however, it is observed that for cases II and III the decay rate of the density fluctuations is almost the same as that of the total r.m.s. velocity. Interpreting ρ'^2 in terms of potential energy (see §3.1.4), this implies that the potential energy decays at almost the same rate as the horizontal components of the kinetic energy for these cases. Significant Reynolds number effects are observed in the figure. For the case with lowest Reynolds number, the decay rate of the scalar after $T = 1$ is faster than for the total r.m.s. velocity. At later times in this case (Case I), the decay rate is even faster than for the non-stratified simulation, consistent with it following decay rate of w'. Recall that **?** and **?** observed that stratification increased the decay rate of velocity, especially the vertical velocity, and so our Case I at later times may provide some insight into the dynamics of those laboratory experiments. This issue will be addressed further in 3.2

3.1.3. *Froude number dependence*

The temporal decay of the horizontal Froude number, defined as $Fr_h = 2\pi\hat{u}_h/\hat{L}_{ux}\hat{N}$, is seen in figure 6 for all three cases. Here $\hat{u}_h$ is the dimensional r.m.s. horizontal velocity and $\hat{L}_{ux}$ is the dimensional analogue of L_{ux}. The decay curves are very similar for all three different Reynolds numbers, although at late time Case I is decaying slightly faster. Furthermore, as suggested by **?**, $Fr_h < \mathcal{O}(1)$ for about $T > 1$, indicating that stratification begins to dominate in this temporal region. This is consistent with the results in figures 3 and 4, where the velocity decay rates and integral scale growth rates change somewhat abruptly near $T = 1$, as the flows enter the strongly stratified regime.

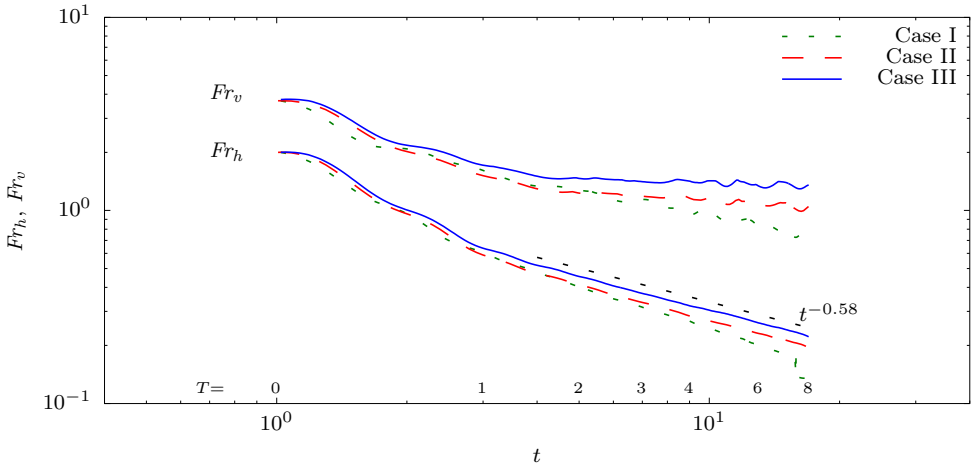

FIGURE 6. Horizontal Froude number Fr_h versus time t.

3.1.4. *Flow energetics*

Information regarding the energy decay rates is given in figure 7. Here E_h is the kinetic energy associated with u and v, and E_v is that associated with w. We define E_p, the potential energy of the density fluctuations relative to the ambient density, as

$$E_p = \frac{1}{2}\left(\frac{2\pi}{Fr}\right)^2 \rho'^2.$$

E_p can be considered as a surrogate for available potential energy (**?**). In panel (a) of the figure, all the energies have been normalised by the local (in time) total energy, i.e., by $E_h + E_v + E_p$. From this panel it is observed that the horizontal components of the kinetic energy become increasingly dominant over the sum of the vertical component and the potential energy. This could be due to one or more of several effects. Possibly internal waves are being absorbed by the more horizontal motions, as in the laboratory experiments of **?**, leading to a decrease in both E_v and E_p while enhancing E_h. Furthermore, as kinetic energy is exchanged with potential energy through the action of the buoyancy flux $-(2\pi/Fr)^2 \langle \rho w \rangle$, with $\langle \cdot \rangle$ denoting a spatial average over the entire domain, the dissipation rate of potential energy χ (see section 3.1.5) provides another avenue for dissipation in addition to the kinetic energy dissipation rate ϵ. From this panel, it is also observed that the partition between the contributions to total energy depends on the Reynolds number, since Reynolds number is the only parameter that is varied between the simulations. This Reynolds number dependence is not surprising. For example, **?** reported, from examining many sources, that the decay exponents for non-stratified turbulence are larger in magnitude for lower Reynolds numbers. Finally, note from panel (b), and the fact that the non-stratified energy decay rate is approximately $t^{-1.1}$, that the decay rate of the total energy is inhibited by the stratification, consistent with the inhibition of the decay rates of the horizontal components of the velocity.

The behaviour of the buoyancy flux for all three stratified cases is seen in figure 8. The oscillations about 0 in the buoyancy flux in figure 8(a) represent net exchanges from the vertical component of the kinetic energy to potential energy (positive values) and back from potential into kinetic energy (negative values), consistent with the plots of these components of the energy. The period of oscillation is about $0.4T_B$ for the case Case I, and appears to lengthen slightly with Reynolds number. These oscillatory results are

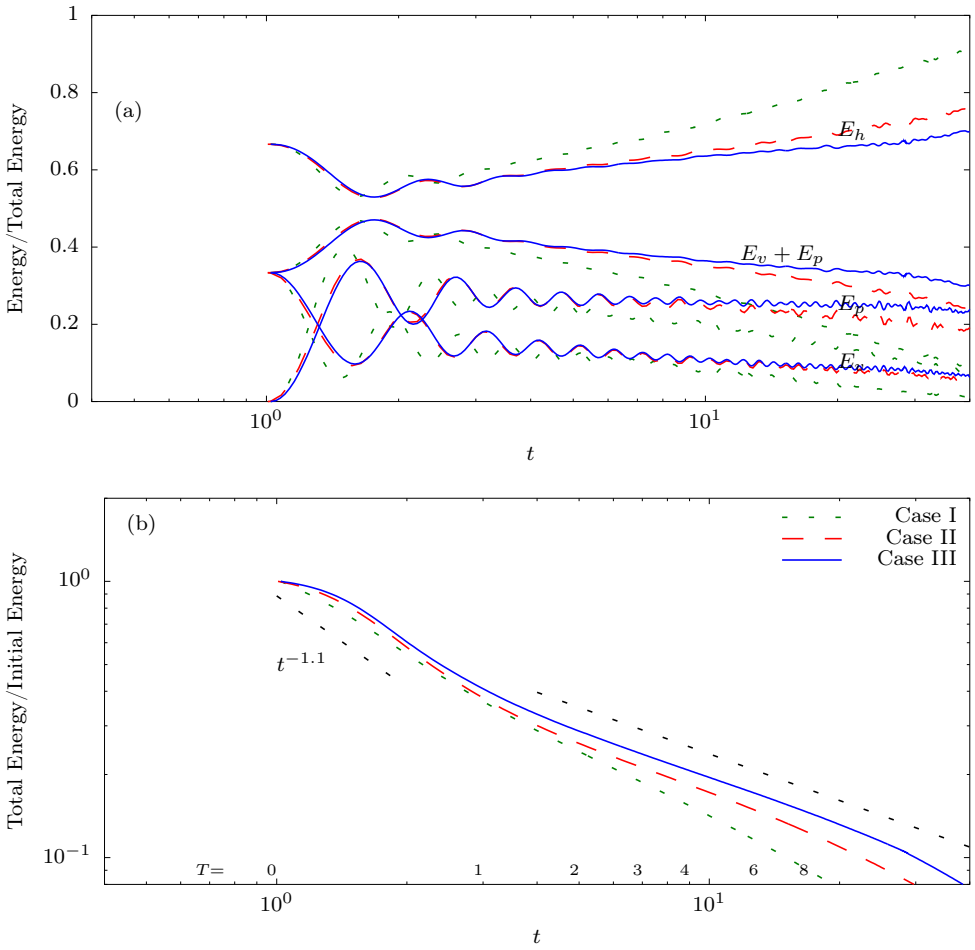

FIGURE 7. (a) Ratio of energy contributions to total energy versus time. (b) Total energy versus time. In places where it is difficult to see the curves for Case II, they almost coincide with those for Case III. In panel (b), the two reference slopes correspond to $n = -0.55$ and $n = -0.28$ on figure 3c.

qualitatively consistent with the numerical simulations of **?** and the laboratory experiments of **?**. Figure 8(b) is a plot of the cumulative (integrated) value of the buoyancy flux, divided by the initial total energy, giving the net transfer of kinetic into potential energy. It is seen that, for cases II and III, the cumulative flux asymptotes to approximately 30% of the initial total energy. Also note that the cumulative flux is somewhat smaller for Case I, the lowest Reynolds number case. These facts are closely related to the behaviour of the mixing efficiency η discussed in the next section.

3.1.5. *Dissipation rates and mixing efficiency*

The dissipation rates of potential and kinetic energies are

$$\chi = \left\langle \frac{2\pi}{Fr^2 PrRe} \nabla\rho \cdot \nabla\rho \right\rangle$$

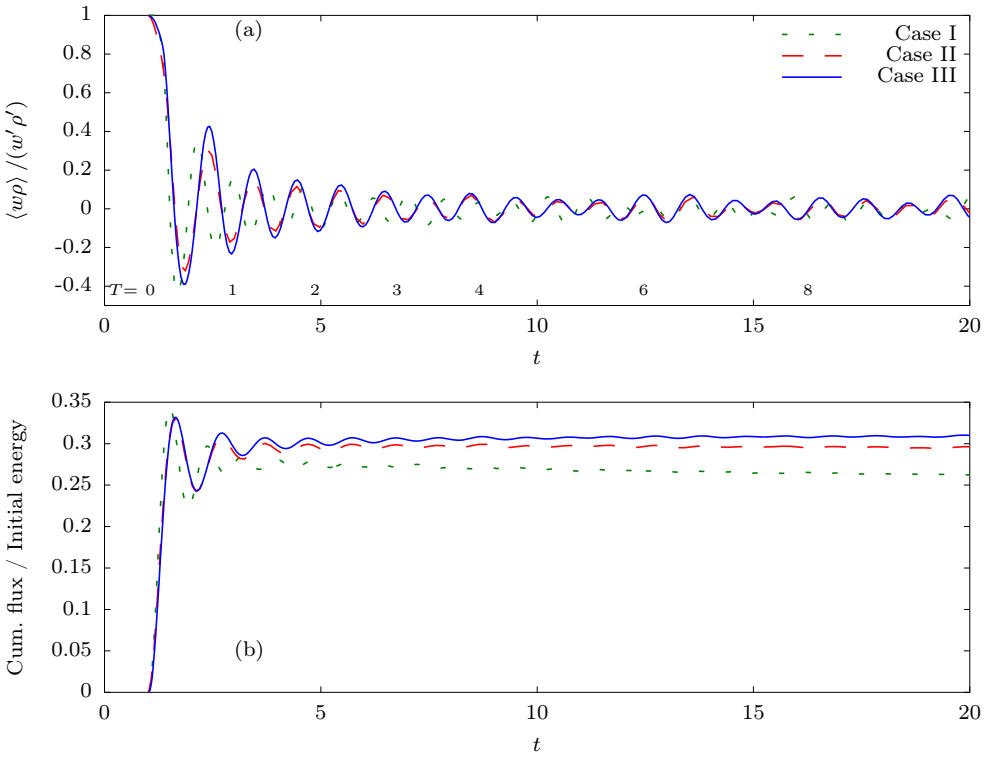

FIGURE 8. (a) Buoyancy flux, normalised by $w'\rho'$, versus time for all three stratified cases. (b) Cumulative buoyancy flux normalised by initial total energy.

and

$$\epsilon = \left\langle \frac{1}{Re} \boldsymbol{S} : \boldsymbol{S} \right\rangle,$$

respectively, where $\boldsymbol{S}$ is the non-dimensional strain rate tensor. The time evolutions of their averages are shown in figure 9. Noticeable is the decrease in ϵ due to the stratification. Furthermore, there is a slight decrease and then increase in ϵ as the Reynolds number is increased, whereas there is a slight increase in χ as it is increased. Also evident is that the non-stratified cases are not quite in power law decay at $t = 1$, which is also apparent in figure 3 for all the non-stratified cases; however power law decay does occur in the non-stratified simulations well before $T = 1$. In addition note that, after the flow adjustment, the ratio of χ to ϵ is about 0.54 except for the lowest Reynolds number case, where the ratio continues to decrease in time. We will find below in §3.2 that, for this lowest Reynolds number case (Case I), the flow might not be fully turbulent beyond about 2 buoyancy periods.

Of special interest is the ratio $\eta \equiv \chi/(\chi + \epsilon)$, which is sometimes taken to be the definition of the mixing efficiency (**??**). From figure 10 it is seen that, for the higher Reynolds number cases, η asymptotes to a value of about 0.35, compared to the value of 0.3 obtained by **?** in a similar regime, to 0.25 obtained by **?** at very low Froude number, to 0.41 inferred from the data of **?**, and 0.17 assumed by **?** based upon ocean data. In the forced homogeneous simulations reported by **?**, η ranges from 0.22 at $Fr_h = 0.22$ (computed in the same way as it is for the current simulations), to 0.37 at $Fr_h = 2.8$.

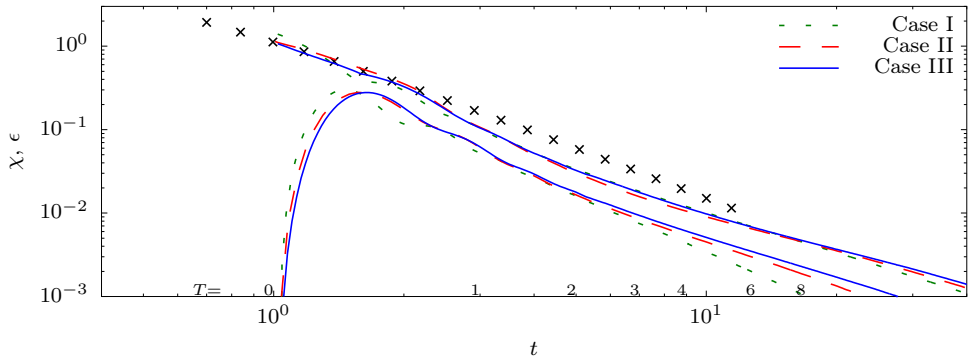

FIGURE 9. ϵ (upper curves), χ (lower curves). Symbols are for Case III with no stratification.

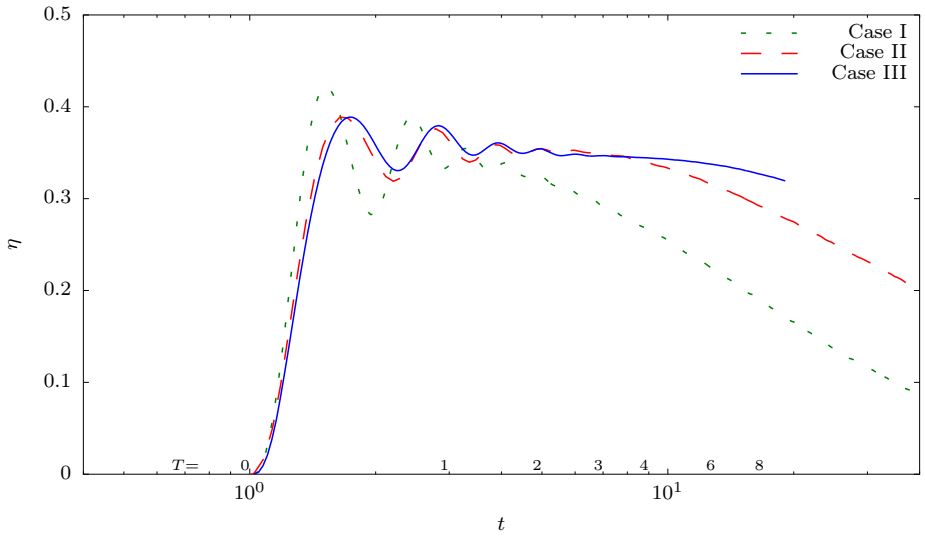

FIGURE 10. Mixing efficiency $\eta = \chi/(\chi + \epsilon)$

Note that the value for η of 0.35 is consistent with the asymptotic ratio of χ/ϵ of about 0.54, as found in figure 9.

There is some evidence that η depends on the Prandlt (or Schmidt) number. For example, from numerical simulations of stratified shear flows, **?** found that η decreased from 0.35 to 0.22 as the Prandlt number increased from 1 to 7. More recently **?** found in numerical simulations of stratified shear flows that η decreased from 0.24 to 0.18 as the Prandlt number increased from 1 to 16. **?** also gave some physical and mathematical reasoning for this decrease with Prandlt number. For a subset of the simulations of **?** run with $Pr = 7$, η ranges from 0.17 at $Fr_h = 0.4$ to 0.28 at $Fr_h = 2.8$.

3.1.6. *The buoyancy Reynolds number and activity parameter*

Dimensional reasoning suggests that three initial parameters are required to describe decaying, homogeneous, stratified turbulence. For equations (2.1), these are chosen to be the Prandtl number, Pr, in addition to the Reynolds and Froude numbers, Re and Fr. The latter are defined here in terms of the integral length scale $\hat{L}$ and r.m.s. velocity $\hat{U}$ of the simulated flow at $t = 1$, *i.e.*, before there is any effect of stratification. The

conditions at $t = 1$ provide a useful basis for non-dimensionalising the flow statistics. To better understand the effects of stable stratification, however, it is useful to consider the local in time values of Re and Fr. Because of the non-isotropy which develops in the flows, the corresponding vertical and horizontal scales in the flow differ significantly, as seen in figure 4. Therefore, considering the local r.m.s. horizontal velocity u_h, one can define two Froude numbers of potential importance, $Fr_h = u_h/NL_{ux}$ and $Fr_v = u_h/NL_{uz}$ based upon the horizontal longitudinal integral scale L_{ux} and the vertical lateral integral scale L_{uz}, respectively. From the scaling arguments of **?**, at least for large Re, it is found that Fr_v should remain $\mathcal{O}(1)$, so that its local in time behaviour need not be considered. Therefore, it is important to locally consider only Re_h and Fr_h, where Re_h is also based upon u_h and L_{ux}. As reviewed in §1, these two parameters combine to form $\mathcal{R} = {Fr_h}^2 Re_h$, whose potential relevance is based on the shearing dynamics observed to occur when strong stratification leads to the tendency for vertical decoupling of horizontal motions (**?**).

In the stratified turbulence literature, $\mathcal{R}$ is often referred to as the 'buoyancy Reynolds number,' a terminology we have adopted in this paper. In the geophysical literature, this terminology usually denotes

$$Gn \equiv \frac{\hat{\epsilon}}{\hat{\nu}\hat{N}^2} = {Fr_t}^2 Re_t \ . \tag{3.1}$$

Here the turbulence Froude and Reynolds numbers, Fr_t and Re_t, are defined in terms of the turbulence length scale $\hat{\ell} = \hat{U}^3/\hat{\epsilon}$, with $\hat{U}$ being the total r.m.s. velocity. These are the definitions used in **?**; however, they refer to Gn as the buoyancy Reynolds number. (Note then that $\mathcal{R}$ and Gn differ in the choice of their characteristic velocity and characteristic length scales.) We use the symbol Gn in deference to the introduction of this quantity by **?**, and to its identification by **?** as a measure of the scale separation available for turbulence between the Ozmidov, $\hat{L}_o = (\hat{\epsilon}/\hat{N}^3)^{1/2}$, and Kolmogorov, $\hat{L}_k = (\nu^3/\hat{\epsilon})^{1/4}$, length scales; we call Gn the 'activity parameter' following some of the early literature on the subject (e.g. **?**).

In figure 11 the evolution of $\mathcal{R}$ and Gn in time are shown. Note that, as seen in terms of their decay rates in figure 11, $\mathcal{R}$ and Gn are not proportional in the present simulations, so that they cannot be used interchangeably. Also note that there is a change in slope in $\mathcal{R}$ at about $T = 1$, consistent with the results for u and v seen in figure 3. It is also apparent that $\mathcal{R}$ scaled by the initial Reynolds number evolves differently for Case I than for Cases II and III. All three cases evolve in a similar manner up to about $T = 2$, at which point Cases II and III appear to diverge from Case I.

Our hypothesis is that the differences in the evolution of the three cases, evident in figure 11, can be explained by when Gn drops below $O(1)$, as will be discussed more in §3.2 on late time results. **?** predicted that $Gn > 30$ is necessary for sustained turbulence, a value supported experimentally by **?**. In simulations of forced homogeneous stratified turbulence with $Gn = 13, 48$, and 220 (**?**), only in the case with $Gn = 220$ is there a range of length scales in which the turbulence is approximately isotropic throughout much of the simulation domain, although all the cases exhibit at least some patches of approximately isotropic turbulence. Even in the case with $Gn = 220$ there is no range of scales consistent with the assumptions of Kolmogorov, Oboukhov, and Corrsin regarding inertial and convective subranges (**???????**). For the same three data sets, **?** find that at $Gn = 220$ the domain is dominated by space-filling patches of turbulence, while when $Gn = 13$ and 48 the simulated flows consist of a mixture of space-filling patches and horizontally-layered turbulence. As seen in figures 1 and 2, the flows studied here become very layered beyond about $T = 2$.

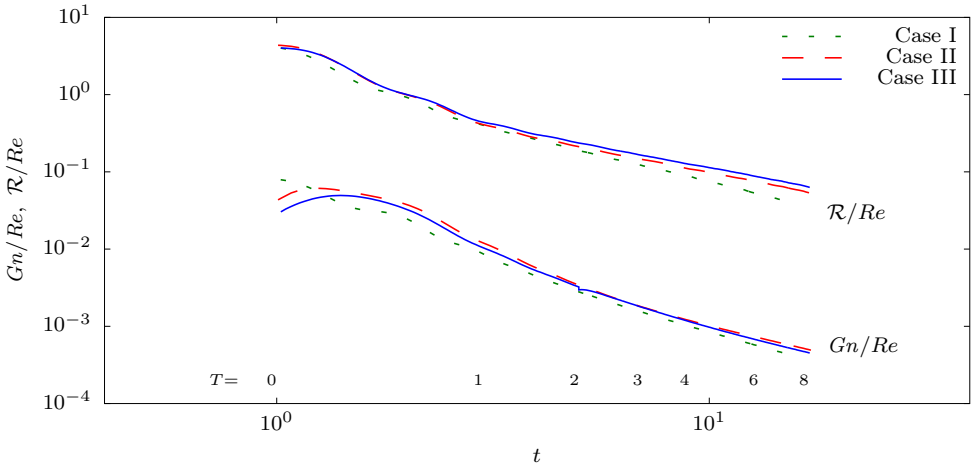

FIGURE 11. $\mathcal{R}$ and Gn, normalised by the initial Reynolds number, versus t.

Turning now to $\mathcal{R}$, **?** have argued that shear instabilities can be expected to occur in the strongly stratified regime provided $\mathcal{R} > O(1)$. This criterion has been verified, to some extent, by the simulations of **?** and refined by **?**. It is seen that, for all the cases and all the times, $\mathcal{R}/Re$ is greater than about 0.1, and so that, approximately, $\mathcal{R} > 15$, indicating that that we would expect shear instabilities to continue to exist for these flows. These instabilities would only be expected to lead to turbulence, however, when approximately $Gn > 0.5$.

? present data from 14 simulations of decaying stratified turbulence that indicate $\mathcal{R} \propto Gn$, but each simulation is sampled at a single time, not as a function of time. For the current simulations, the plots of $\mathcal{R}$ and Gn versus time in figure 11 indicate that Gn decays more rapidly than does $\mathcal{R}$ for all three cases; therefore there is no proportionality between Gn and $\mathcal{R}$ and, in all three cases, the ratio $\mathcal{R}/Gn$ increases with time. The ratio of Gn to $\mathcal{R}$ is closely related to the ratio of the integral to the turbulence length scales, L_h and $\ell = u_{rms}^3/\epsilon$, *i.e.,* the ratio

$$\mathcal{D} \equiv \epsilon L_h / u_{rms}^3 \,. \tag{3.2}$$

To be precise, $Gn/\mathcal{R}$ includes a factor of the ratio of the r.m.s. horizontal velocity to the r.m.s. total velocity, and there is an additional factor of $2\pi^2$. $\mathcal{D}$, however, is well known in the study of nonstratified turbulence and so we turn our attention to it rather than $Gn/\mathcal{R}$. **?** shows that, when the ratio is computed from a model spectrum, it depends on the Reynolds number over the range of Reynolds numbers accessed by all but a few numerical simulations and laboratory experiments in homogeneous, isotropic turbulence. From an examination of results from a number of laboratory experiments and numerical simulations, **?** reports $\mathcal{D}$ in the range of about 0.4 to 1.81. He also notes that simulations of homogeneous, isotropic turbulence by multiple researchers can be divided into two groups, with $\mathcal{D}$ for one group of simulations being consistent with each other but markedly higher than for the other group, for which $\mathcal{D}$ is consistent with the analysis of Pope. For decaying homogeneous stratified simulations, **?** report $\mathcal{D}$ as low as 0.3. **?** report $\mathcal{D} \approx 0.4$ for their snapshots of the 14 decaying cases referenced above. For the simulations of forced stratified turbulence with $Gn = 13$, 48, and 220, **?** reports $\mathcal{D} = 0.53$ at $Gn = 220$ and 0.57 at $Gn = 13$. Sreenivasan reports that $\mathcal{D}$ tends to be higher for forced cases. We note that typically in forced simulations, and certainly in those of **?**, the large scales are

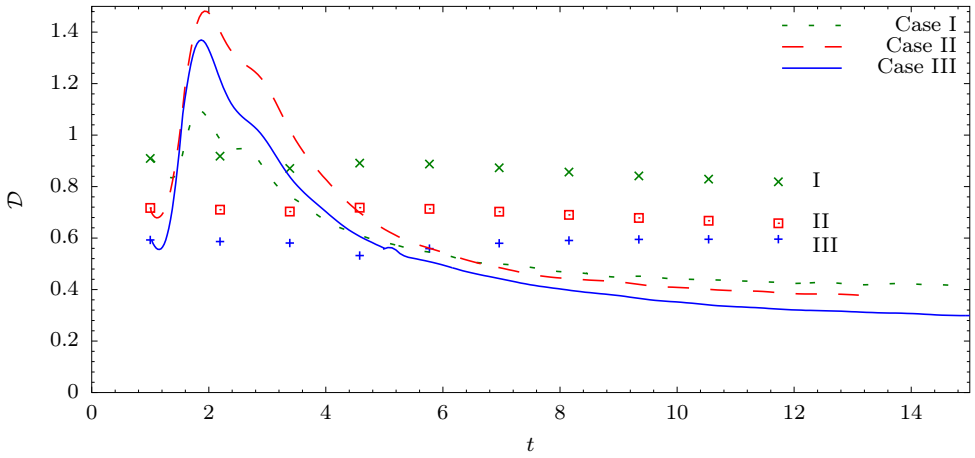

FIGURE 12. Length scale ratio.

not as well resolved as in decaying simulations, which adds to the difficulty in accurately estimating L_h.

Data for $\mathcal{D}$ for the current simulations are shown in figure 12. For the non-stratified cases, the values are consistent with those collected by **?**, and they exhibit the expected trend of increasing with decreasing Reynolds number from one simulation to the next. The results for the stratified cases go through an adjustment period at early time and then trend toward the range 0.3 to 0.4, consistent with the decaying cases of **?** and **?**. The lower values of $\mathcal{D}$ for the stratified cases are consistent with the decrease in ϵ and the increase in both u_h and L_h.

3.1.7. *Energy spectra*

The horizontal velocity spectra E_{xx} versus horizontal wave number κ_x are plotted in figure 13(a), where the spectra of u has been averaged with that of v. The corresponding compensated horizontal spectra versus horizontal wave number times the Kolmogorov length scale L_k are plotted in figure 13(b). It is seen that, at $T = 0.0$, when the stratification is applied, the non-stratified spectrum has a moderate inertial range. The compensated spectrum in figure 13(b) is consistent with the Kolmogorov constant of about $C_1 = 0.53$, which is slightly higher than the value of 0.49 in **?** but well within the range for the many data sets reviewed by **?**.

In isotropic turbulence at high enough Reynolds numbers, there is found a bump in the compensated spectrum to the right of $\kappa L_k \approx 0.02$, which is sometimes attributed to a "bottleneck" of energy transferring to smaller scales. **?** review efforts to understand and model this phenomenon. **?** shows that stratification suppresses this bump and that the -5/3 slope can occur at the top of the dissipation range even though it does not occur in the inertial range. The suppression of the bump by stratification is consistent with the hypothesis that the bump is due to the bottlenecking of the energy transfer rate combined with the observation that, for the current simulations, stratification reduces the energy decay rate, and hence the energy transfer rate.

Note that in figure 13(b) there is a bottleneck bump to the right of $\kappa L_k \approx 0.02$ at $T = 0$. By $T = 0.5$ the bump has been suppressed and a peak in the spectrum has begun to develop in the range where the inertial-range plateau exists at $T = 0$. By $T = 1.2$, the spectrum is very similar to those in figure 4(a) of **?**. This is somewhat surprising because

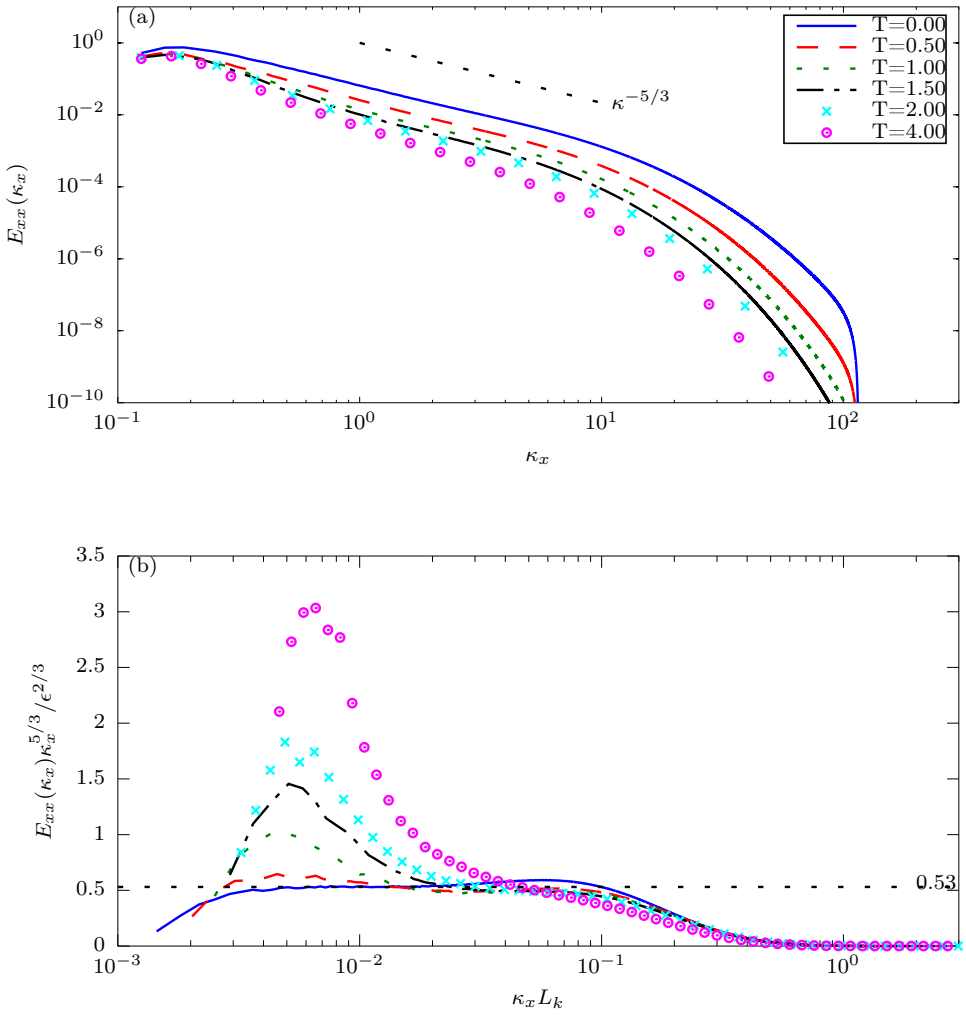

FIGURE 13. Uncompensated (a) and compensated (b) longitudinal spectra of u averaged with that of v.

it has been assumed that the peak in the spectra is an artefact of the energy forcing used to maintain the statistical stationarity of those simulations, yet in the current simulations there is no forcing. The plots of the compensated horizontal spectra are also qualitatively similar to those obtained by **?**, and in fact the growth of the spectra in the low wave number region, and the decay in the high wave number region, are also consistent.

The question arises regarding whether a stratified turbulence inertial range, as proposed by **?**, should be expected for our simulations.The possibility for this to occur will depend upon (i) the ratio of the energy-containing range scale, characterized by L_h, to the Ozmidov scale L_o; and (ii) the ratio of the Ozmidov scale to the Kolmogorov scale, given by $Gn^{4/3}$. A stratified turbulence inertial range would be expected to exist between

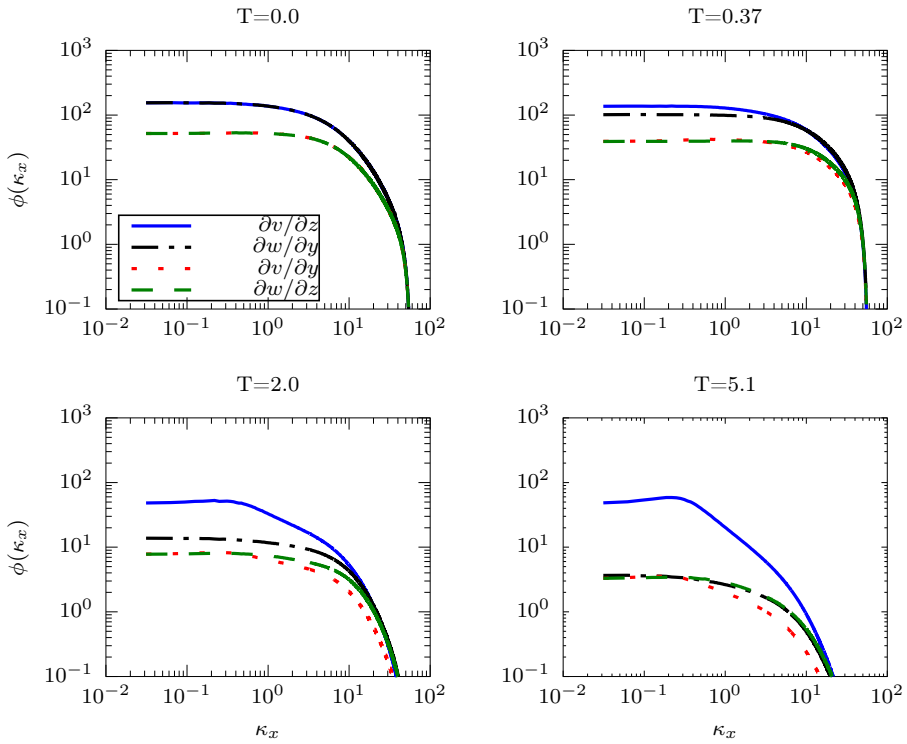

FIGURE 14. Horizontal spectra of various shear terms.

the energy-containing and Ozmidov wave numbers, so that L_h/L_o should be at least 100 or more. Furthermore, for turbulent behaviour to exist, we find in §3.2 that Gn must be at least of order 1. Considering the highest Reynolds number case (Case III), we find that at $T = 1$, where the flow becomes strongly affected by stratification, $L_h/L_o = 32.3$, while $L_o/L_k = 10.1$. Clearly the ratio of L_h/L_k is not large enough for an inertial range to exist. When the ratio of L_h/L_o becomes large enough for the inertial range to exist, at $T = 6$, where $L_h/L_o = 216$, then L_o/L_k has dropped to 1.4, which is too small to expect active turbulence. Therefore we conclude that there is not enough separation of scales for a stratified flow inertial range to occur. The flow would have to be started at a substantially higher Reynolds number for the possibility to exist.

Some additional insight into the dynamics of strongly stratified flows can be seen from examining the horizontal spectra of various components of the velocity gradient tensor. Figure 14 contains plots of the k_x spectra of $\partial v/\partial z$, $\partial w/\partial y$, $\partial v/\partial y$, and $\partial w/\partial z$ for four points in time for Case III, the highest Reynolds number case. Note that, for isotropic turbulence, it is expected that the spectra of $\partial v/\partial z$ and $\partial w/\partial y$ will be identical, as will the spectra of $\partial v/\partial y$, and $\partial w/\partial z$. It is clear that at $T = 0$ this is the case. As the flow evolves, the spectra of $\partial v/\partial y$, and $\partial w/\partial z$ remain approximately the same, although the spectrum of $\partial v/\partial y$ decreases slightly faster than that of $\partial w/\partial z$ at higher wave numbers. This supports the scaling arguments of **?** that all three terms in the continuity equation, $\partial u/\partial x$, $\partial v/\partial y$, and $\partial w/\partial z$, should be of the same order. Somewhat surprisingly, the spectra of $\partial w/\partial y$ and $\partial w/\partial z$ become almost identical at the latest time. What is noteworthy, however, is the rapid decrease with time of the spectra for $\partial w/\partial y$, $\partial v/\partial y$, and $\partial w/\partial z$ compared to that for $\partial v/\partial z$, with the spectrum for $\partial v/\partial z$ evolving

well above the rest. Furthermore, the peak in the spectrum of $\partial v/\partial z$ remains into smaller wave numbers. Both of these facts are indications of the development of strong vertical shearing of the horizontal motions as suggested by **?**.

3.2. *Late time results*

We now consider the late time behaviour of these flows, when Gn falls to $\mathcal{O}(1)$ and below, and so viscosity becomes a dominating influence. Figure 15 contains plots of u', w' and $E_p^{1/2}$ versus time carried out to 150 buoyancy periods or more for each case, and where Gn has dropped to values of 0.01 or less at very late times. Note the Gn scale at the bottom of each plot, depicting the local values of Gn at different times for each case. There are two things to note about these plots. First, for each case, between values of Gn of 1 and 0.1, u' begins to decay at a slightly steeper rate. Second, for values of Gn in this same range, the vertical velocity and $E_p^{1/2}$ (proportional to ρ') begin to decay precipitously, indicating that the flows are becoming quasi-horizontal.

These plots can be better understood by examining the trajectory of each flow in the Fr_h-Gn plane, as given in figure 16. Each flow is seen to go through three regimes. In the first, the flows decay at the non-stratified rate, which is seen in figure 3 to occur up to about 1 buoyancy period after flow initiation, when the values of the local Froude numbers have fallen to about 0.6 (see figure 6). We take this to be the value of Fr_h when a flow has entered the strongly stratified regime. The decay rate in this regime diminishes due to the effects of stable stratification, approximately as predicted by **?**. Finally, in the third regime, when Gn has decayed to between 1 and 0.1 for each case, the flows become viscously dominated and begin to decay at a faster rate. Note that this viscous domination had already been observed for Case I at earlier times in the behaviour of ρ' in figure 5, in the behaviour of the various components of energy in figure 7(a), and in the behaviour of the mixing efficiency in figure 10.

These results are analogous to those obtained in the experiments of **?** discussed in §1. He studied the decay of turbulence in the wake of a towed sphere in a salt-stratified towing tank, and found in measuring the mean axial velocity that, initially, the flow decayed at the non-stratified rate. But at a time of the order of a buoyancy period, the decay rate decreased appreciably in what he called the non-equilibrium regime. Further in time, in the region he called the late wake, or quasi-two-dimensional regime, the flow again decayed at a faster rate. We speculate that in this last regime Gn had become small in his flows, which would therefore be viscously dominated. Furthermore the vertical velocity had been suppressed compared to the horizontal velocity, as the flow exhibited a quasi-horizontal vortex structure.

Additional insight can be gained by examining the behaviours of the Froude numbers, based upon the horizontal and vertical integral scales, throughout the flow decay, as shown in figure 17. The Froude number based upon the horizontal integral scale, Fr_h, is seen to continually decay, although the decay is somewhat diminished when the effects of stratification become strong, and then the decay becomes stronger as viscous effects begin to dominate. At first the Froude number based upon the vertical scale, Fr_v, begins to decay at a rate similar to that of Fr_h. As the effects of stratification become strong, however, Fr_v becomes approximately constant, as predicted by the scaling arguments of **?**, and as seen in the simulations of **?**. As the effects of viscosity begin to dominate, then Fr_v begins to decay.

Based upon our simulation results, we find that it is most useful and instructive to divide up the flows into three different regimes, depending upon the values of Fr_h and Gn. When $Fr_h > \mathcal{O}(1)$ the flows behave almost as non-stratified flows and we term this regime the weakly stratified regime. When Fr_h becomes less than $\mathcal{O}(1)$, in our case

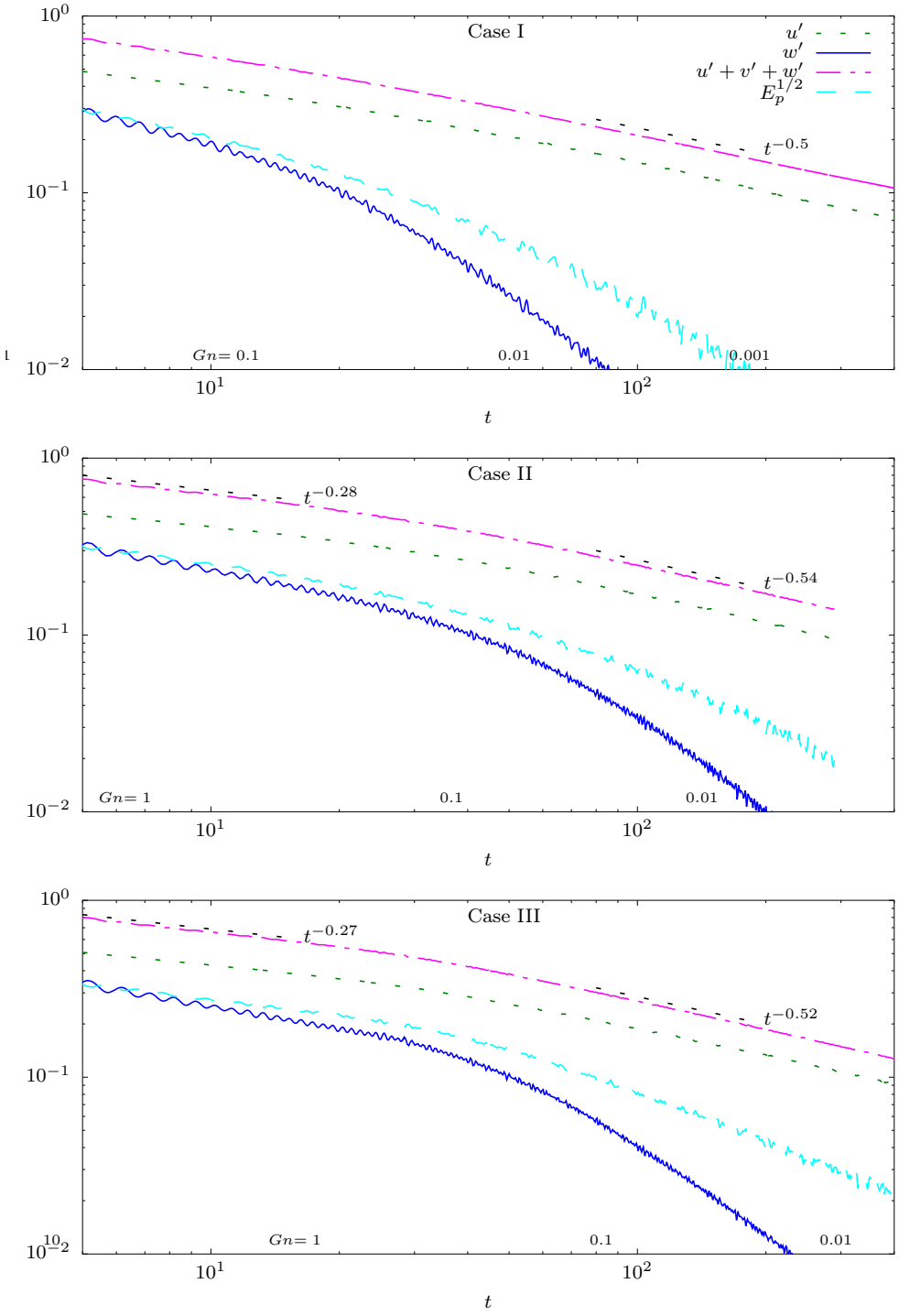

FIGURE 15. Evolution of u', v', w' and $E_p^{1/2}$ into late time. Reference slopes are shown for $Gn > 1$ and $Gn \ll 1$ except for Case I $Gn > 1$ for which is not in the range of times on this figure. For velocity data at early times see figure 3.

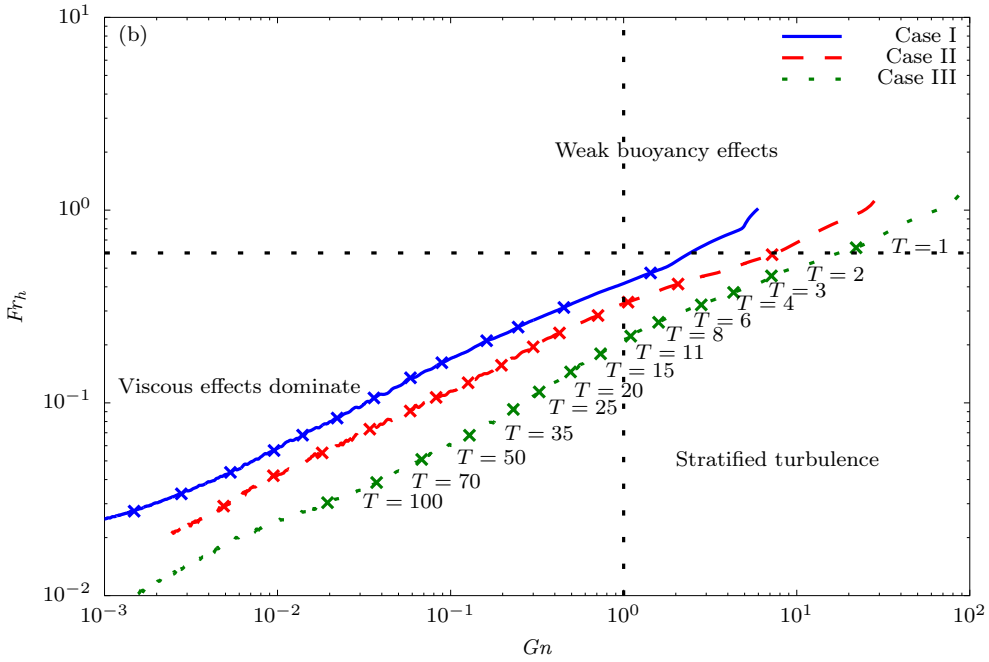

FIGURE 16. The trajectory of each flow in the Fr_h-Gn plane. The symbols mark the time in buoyancy periods, with the corresponding times indicated on the curve for Case III.

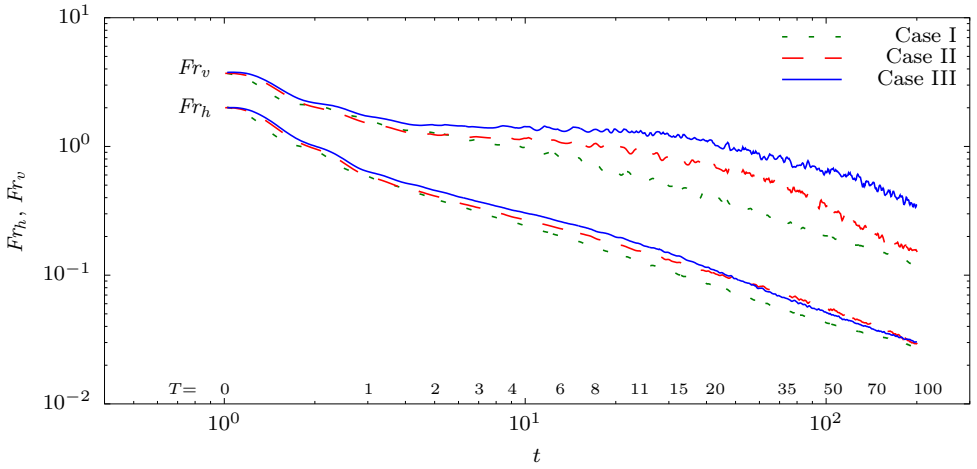

FIGURE 17. Froude numbers.

less than about 0.6 which occurs at about one buoyancy period, stratification begins to strongly affect the flows, and we term this the strongly stratified regime, as discussed in the Introduction. Depending on the local value of Gn, the strongly stratified regime splits into two parts. When Gn is greater than $\mathcal{O}(1)$, the flow obeys the decay laws predicted by **?**, and the scaling arguments predicted by **?**, and we call this the stratified turbulence regime, in deference to the terminology introduced by **?**. Finally, in the strongly stratified regime, when Gn has dropped somewhat below 1, the flows become quasi-horizontal, and

the dissipation rate is approximately governed by the vertical shearing of the horizontal velocity, and we refer to this as the viscous-dominated regime.

The behaviour of the flow in this late time, viscous-dominated regime can be seen from the scaling arguments of **?**, as modified by **?** to include the effects of viscosity. The arguments suggest that the ratio of the r.m.s. vertical velocity to the r.m.s. horizontal velocity should be proportional to Fr_h/Fr_v, so that the flow should be quasi-horizontal in this regime. **?** also argued that as Gn becomes small, the vertical viscous term in the horizontal momentum equation becomes large compared to the vertical transport term, suggesting that the vertical integral scale behaves as $L_v = L_h Re^{-1/2}$. Furthermore, neglecting the vertical transport term, and assuming that the aspect ratio L_v/L_h is small as suggested by the scaling arguments and by figure 17, so that the horizontal diffusion terms can be neglected, the result is that (2.1) reduce to

$$\frac{\partial}{\partial t}\vec{u} + \vec{u}_h \cdot \nabla_h \vec{u}_h = -\nabla_h p + \frac{1}{Re}\frac{\partial^2 \vec{u}_h}{\partial z^2} \tag{3.3a}$$

$$0 = -\left(\frac{2\pi}{Fr}\right)^2 \rho - \frac{\partial p}{\partial z} \tag{3.3b}$$

$$\nabla_h \cdot \vec{u}_h = 0 \tag{3.3c}$$

$$\frac{\partial \rho}{\partial t} + \vec{u}_h \cdot \nabla_h \rho = \frac{1}{RePr}\frac{\partial^2 \rho}{\partial z^2} \tag{3.3d}$$

There are several indications of the appropriateness of these equations to describe the late-time behaviour of flows with small Gn. One is the fact that the flows are approximately horizontal, i.e., u', $v' \gg w'$, which in the present case is clearly indicated in figure 15. Another indication can be found by examining the ratios

$$Rt_G = \frac{15\nu}{4\epsilon}\left\langle \left(\frac{\partial u}{\partial z}\right)^2 + \left(\frac{\partial v}{\partial z}\right)^2 \right\rangle \tag{3.4a}$$

$$Rt_D = \frac{15\nu}{2\epsilon}\left\langle \left(\frac{\partial u}{\partial x}\right)^2 + \left(\frac{\partial v}{\partial y}\right)^2 \right\rangle \tag{3.4b}$$

$$Rt_H = \frac{15\nu}{4\epsilon}\left\langle \left(\frac{\partial u}{\partial y}\right)^2 + \left(\frac{\partial v}{\partial x}\right)^2 \right\rangle \tag{3.4c}$$

$$Rt_M = \frac{15\nu}{4\epsilon}\left\langle \left(\frac{\partial w}{\partial x}\right)^2 + \left(\frac{\partial w}{\partial y}\right)^2 \right\rangle \tag{3.4d}$$

$$Rt_V = \frac{15\nu}{\epsilon}\left\langle \left(\frac{\partial w}{\partial z}\right)^2 \right\rangle \ . \tag{3.4e}$$

For (3.3) to have near validity, Rt_G must be approximately 15/4. In contrast, in isotropic turbulence, all of the preceding ratios should be unity. Both of these conditions are observed in figure 18, which shows the ratios for case II. At early times, each of the ratios is approximately unity whereas at late time Rt_G appears to by asymptoting to 15/4.

The results from other studies exhibit this behaviour of the dissipation rate as well. Both **?** and **?** performed experiments in salt-stratified tanks, and both generated turbulence by towing a vertical grid through the tank. At the later stages of decay in both experiments the value of Gn had dropped to values well below one. In addition, the flows had become approximately horizontal, and in both experiments it was reported that the

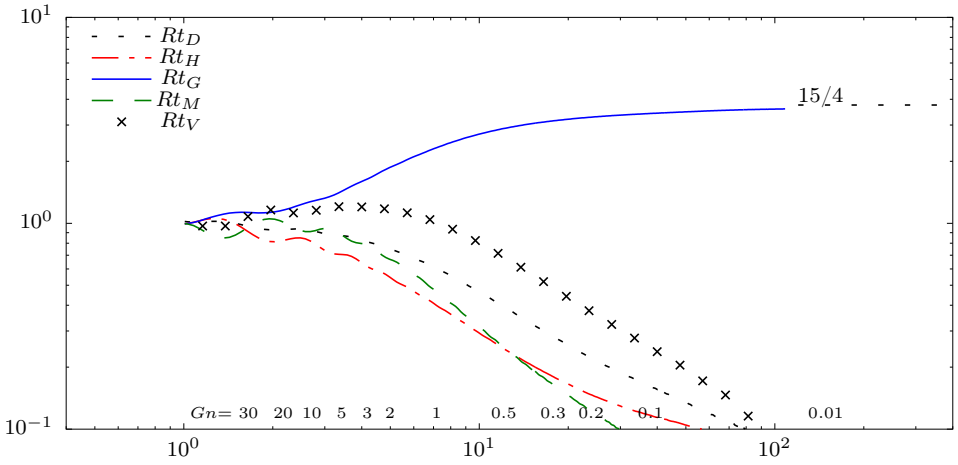

FIGURE 18. Plot of the five statistically independent contributions to ϵ, normalised as in (3.4), for Case II.

ratio Rt_G was well above 0.9. These features for both experiments all indicate the approximate validity of (3.3) at later times. **?** performed direct numerical simulations in a strongly stratified fluid of the decay of flows initially consisting of Taylor-Green vortices, similar to the work of **?**, but over a very broad range of Reynolds number, Froude number, and Gn. They found that the ratio Rt_G is a very strong function of Gn, and that Rt_G being near 0.9 only occurred when Gn was order one or less. From the present results, and from these experimental and numerical results, there is reason to speculate that (3.3) hold in many other flows that are strongly stratified and Gn is small.

4. Conclusions and Discussion

Direct numerical simulations were used to study the effects of stable ambient density stratification on initially isotropic turbulence. To initialise the stratified flows, and for comparison with cases with stratification, first of all three non-stratified cases were run at three different Reynolds numbers. It was found that all three flows attained approximately self-similar decay, with r.m.s. decay rates of approximately $t^{-0.56}$, and integral scale growth rates of approximately $t^{0.44}$. These values are not far from the rates of $t^{-0.6}$ and $t^{0.4}$ predicted for Saffman turbulence (**?**), and observed in some laboratory data. Therefore, these non-stratified cases are useful for the initialisation of and comparison with the cases with stratification.

In the cases with stable stratification, analogous to the results of **?**, as the flows decay we find that they traverse three different regimes which depend on the local Froude number, Fr_h, and activity parameter, Gn. In the first regime, the weakly stratified regime, which occurs up to approximately one buoyancy period, when Fr_h is above about 0.6, the flows follow their non-stratified counterparts. By about one buoyancy period, however, the flows have adjusted to the stable stratification as the value of F_h falls below 0.6. If Gn remains high enough, then the flows enter the second regime, which we term the stratified turbulence regime, and proceed to decay in a manner similar to that predicted by **?**, and to satisfy the scaling analysis of **?**. In particular, the horizontal r.m.s. velocity decay rates are reduced, the growth rates of the horizontal integral scales of the horizontal velocities increase, while the vertical integral scales of the horizontal velocities begin to decrease. Finally, when the activity parameter decays to a value in the range of 0.1 to

1, the flows enter into the third regime, the viscous dominated regime. Here the flow dynamics have changed considerable and follow the scaling analysis of **?**. In particular the vertical velocity becomes very small compared to the horizontal velocities, and the kinetic energy dissipation rate is dominated by the vertical shearing of the horizontal motions.

The results regarding the decrease in decay rate in the stratified turbulence regime are at least qualitatively consistent with the data from several laboratory experiments (**????**). They are inconsistent, however, with the results of several other laboratory experiments (**???**). It is not clear why our results differ from some of the experimental results, and why in fact some of the experimental results differ from one another while performed under seemingly similar conditions. As mentioned in the introduction, a key difference between our simulations and the laboratory experiments is how the flows are initialised. Our flows have achieved close to a classical isotropic, homogeneous, decaying turbulent flow before the stratification is imposed. On the other hand in the laboratory experiments the stratification exists before the turbulence is generated. Generally in the laboratory experiments where a grid of mesh size M is used to generate the turbulence, a certain distance from the grid, say x_0/M, is required before the flow begins to decay in a self-similar manner. Taking U to be the speed of the grid relative to the fluid, and with $t_0 = x_0/U$ as the time it takes for the flow to become self-similar, then, in terms of buoyancy periods, this is $Nt_0/2\pi = (x_0/M)(NM/2\pi U) = (x_0/M)/Fr$. In many of the laboratory experiments, $Fr \sim (x_0/M)$, suggesting that the flows are often modified by stratification before they begin self-similar decay. These facts would suggest a change in decay behaviour different from what is obtained in our simulations; but it would not indicate how the decay rates would be different.

There are several interesting features of the flows in the stratified turbulence regime. For example, the vertical component of the kinetic energy decays at a faster rate than the two horizontal components while, after its initial adjustment, the density fluctuation ρ' decays at approximately the same rate as does u_h. From an energetics perspective, this indicates that the potential energy decays at approximately the same rate as the horizontal components of the kinetic energy. This could be due to the density field trying to stay in cyclostrophic adjustment with the horizontal components of the velocity field. Another feature of this regime is the behaviour of the local Froude numbers; the Froude number Fr_h continues to decay, while Fr_v becomes approximately constant, consistent with the predictions of **?**. Furthermore, in the stratified turbulence regime, for the two higher Reynolds number cases, the mixing efficiency asymptotes to approximately 0.35. This is roughly consistent with a number of numerical simulations with $Pr = \mathcal{O}(1)$ (**????**). The lowest Reynolds number case is only briefly in the stratified turbulence regime, however. After about 2 buoyancy periods its activity parameter has dropped well below 1 as it enters the viscous-dominated regime; its mixing efficiency as well as F_v begin to decay.

The horizontal spectra of the horizontal components of the velocity behave very differently in the stratified cases compared to the non-stratified cases. Initially the spectra for these flows have a moderate inertial range, with a bump in the compensated spectra sometimes attributed to a "bottleneck" in the energy transfer to smaller scales. As each flow evolves into the stratified turbulence regime, however, a peak in the compensated spectra arises and continues to grow at about wave number $\kappa_x L_k = 8 \cdot 10^{-3}$. In addition, in examining the horizontal spectra of various shear terms, it is found that the spectra of $\partial u/\partial x$, $\partial v/\partial y$, and $\partial w/\partial z$ evolve in a very similar manner, again supporting the scaling arguments of **?**. Even at moderate times the vertical shearing of the horizontal compo-

nent of the velocity at somewhat low wave numbers begins to dominate, indicating that vertical shear layers are probably driving the turbulence.

When Fr_h is below 0.6 and the value of Gn drops below between 1 and 0.1, the flows enter the third regime, the viscous-dominated regime. Here the flow dynamics change again. Now the horizontal components of the velocity decay at a faster rate, similar to the decay rate in the first regime. In addition, the vertical velocity and density fluctuations decay at a much faster rate, as the flow becomes approximately horizontal. In this viscous dominated regime, the flow behaviour appears to be consistent with (3.3), based upon the scaling arguments of **?**.

It should be mentioned that, as listed in Table 1, a fourth case was simulated, Case IV, with the same initial Reynolds number as Case III, but with a different initial Froude number, in this case $Fr_h = 1$. This would possibly allow the examination of the effect of the initial Froude number, and would permit the flow to enter into the stratified turbulence regime earlier in time and so more energetic. Since the activity parameter is proportional to $1/\hat{N}^2$, however, when the flow for Case IV enters into the stratified turbulence regime, its Froude number Fr_h and activity parameter Gn have almost identical values as for Case III, so that the flow behaviour was very similar to that of Case III. Therefore the results for Case IV are not presented.

Acknowledgements

This work was funded by the Office of Naval Research via grant N00014-12-1-0583. High performance computing resources were provided through the U.S. Department of Defense High Performance Computing Modernization Program by the Army Engineer Research and Development Center and the Army Research Laboratory under Frontier Project FP-CFD-FY14-007.